

Atomistic details of the Catalytic Mechanism of Fe(III)–Zn(II) Purple Acid Phosphatase

Marta E. Alberto,[†] Tiziana Marino,[†] Maria J. Ramos,[‡] and Nino Russo^{*,†}

Dipartimento di Chimica, Università della Calabria, Via P. Bucci, cubo 14c, 87036 Arcavacata di Rende (CS), Centro di Calcolo ad Alte Prestazioni per Elaborazioni Parallelle e Distribuite—Centro d’Eccellenza MIUR, Italy and REQUIMTE, Departamento de Química, Faculdade de Ciências, Universidade do Porto, Rua do Campo Alegre, 687, 4169-007 Porto, Portugal

Received April 08, 2010

Abstract: In the present work, we performed a theoretical investigation of the reaction mechanism of the Fe(III)–Zn(II) purple acid phosphatase from red kidney beans (rkbPAP), using the hybrid density functional theory and employing different exchange–correlation potentials. Characterization of the transition states and intermediates involved and the potential energy profiles for the reaction in different environments (gas phase, protein environment, and water) are reported. Our results show that the Fe(III)–Zn(II)PAP catalyzes the hydrolysis of methylphosphate via direct attack by a bridging metals-coordinated hydroxide leading to the cleavage of the ester bond. From our study emerges that the rate-limiting step of the reaction is the nucleophilic attack followed by the less energetically demanding release of the leaving group. Furthermore, we provide insights into some important points of contention concerning the precatalytic complex and the substrate coordination mode into the active site prior to hydrolysis. In particular: (i) Two models of enzyme–substrate with different orientations of the substrate into the active site were tested to evaluate the possible roles played by the conserved histidine residues (His 202 and His 296); (ii) Different protonation states of the substrate were taken into account in order to reproduce different pH values and to verify its influence on the catalytic efficiency and on the substrate binding mode; (iii) The metals role in each step of the catalytic mechanism was elucidated. We were also able to ascertain that the activation of the leaving group by the protonated His 296 is decisive to reach an optimal catalytic efficiency, while the bond scission without activation requires higher energy to occur.

1. Introduction

Purple acid phosphatases (PAPs)^{1–3} belong to binuclear metallohydrolases, an interesting family of enzymes that have received in the last years considerable attention.^{4–11} Binuclear sites in enzymes appear to have several potentially useful properties, not found in mononuclear centers, which play essential roles in catalysis. Members of this class have been recognized as potential targets for the development of chemotherapeutics and for drug design against a wide variety

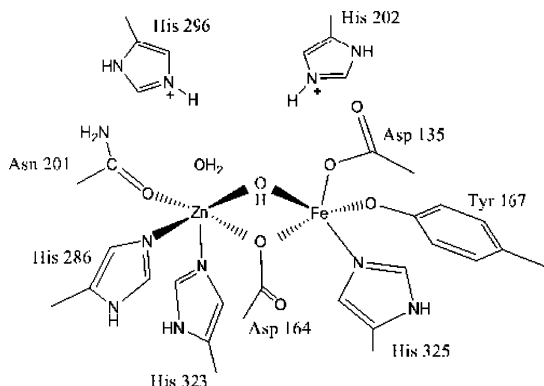
of human disorders^{12–20} and represent also promising candidates in bioremediation.²¹

PAPs are the only binuclear metallohydrolases that use a heterovalent active site Fe(III)–M(II) to catalyze the hydrolysis of monophosphates at acidic to neutral pH.^{1–3,22–26} The identity of the divalent metal ion varies with the source of the enzyme. Mammalian PAPs contain an antiferromagnetically coupled binuclear iron center Fe(III)–Fe(II) in the active site,^{27–33} while plant PAPs most typically have Fe(III)–Zn(II) centers,^{26,34–36} but an interesting example of an enzymatically active binuclear Fe(III)–Mn(II) center was found in the case of PAP from the sweet potato.^{24,25,37} In spite of the scarce similarity in their primary sequences, the

* Corresponding author. E-mail: nrusso@unical.it.

[†] Università della Calabria.

[‡] Universidade do Porto.

Scheme 1. Red Kidney Bean PAP Active Site

active site structure and the residues coordinating the metal ions in the active site are identical in mammalian and plant PAPs, displaying similar enzymatic and spectroscopic properties.³⁸ For example, the intense purple color that distinguishes PAPs from the other phosphatases is due to a charge-transfer transition ($\lambda_{\text{max}} = 510\text{--}560\text{ nm}$) in the active site from a conserved tyrosinate to the Fe(III) ion.^{39–41} Nevertheless, while plant PAPs have a chromophoric center similar to that of their animal counterparts ($\lambda_{\text{max}} = 550\text{ nm}$), their activity cannot be regulated by reversible oxidation/reduction, as it indeed occurs for mammalian PAPs which are reversibly inactivated by the oxidation of the divalent iron ion, suggesting that PAP may be regulated by changes in redox potential within animal cells.^{42,43} The identity of their active sites has been demonstrated in several studies by using metal ion replacement^{44–52} and by spectroscopic and magnetochemical measurements,^{53,54} giving evidence that they employ a similar working mechanism. Moreover other studies suggest that rkbPAP is a good model for the structure and mechanism of other acid phosphatases, such as the human one.⁵⁷ PAP from red kidney beans, the object of our investigation, was the first member of this family for which a crystal structure became available^{55,56} and is by far the most explored so far. The metal atoms first-shell ligands include seven invariant aminoacid residues: three histidines, two aspartates, a tyrosine, and an asparagine (Scheme 1).⁵⁶ The presence of the water molecule terminally coordinated to the divalent metal ion was supported by ENDOR measurements⁵⁸ as well as electron density maps,^{59,60} and EXAFS⁶¹ studies sustained the presence of the bridging hydroxide, the most likely candidate as the nucleophile.⁵⁸ Although in many earlier studies the presence of a terminal Fe(III)-bound water molecule as a nucleophile candidate has been proposed,^{62–64} ENDOR measurements of pig PAP and rkbPAP–SO₄ crystal structures indicate that there is no water ligand at the iron site, suggesting also that the trivalent metal ion is five coordinated.⁵⁸ Such evidence lead to the exclusion of a mechanism in which a terminal Fe(III)-bound hydroxide acts as nucleophile. Moreover, experimentally it was observed that the reduced nucleophilicity of the bridging hydroxide is compensated by an increased electrophilicity of the substrate when comparing the possibilities of: (i) a terminally coordinated nucleophile and terminally coordinated substrate, with (ii) a bridging nucleophile and bridging substrate.⁵⁸ In addition, the crystal structures of PAPs,

determined in the presence of a phosphate group,⁵⁶ show a network of hydrogen bonds with uncoordinated and conserved histidine residues of the second shell of the ligands (His 202 and His 296 for rkbPAP), which, therefore, could play essential roles in catalysis. Although the importance of these conserved histidines has been demonstrated by site-directed mutagenesis studies,^{14,65,66} it is still not clear the effective role of each one in the stabilization of the substrate in the catalytic cavity.

Despite the presence in the literature of structural spectroscopic and kinetic data, the individual steps of the PAPs-catalyzed hydrolysis reaction remain a matter of controversy. The general mechanism proposed in the literature for PAP-catalyzed reactions involves a nucleophilic attack performed by the bridging hydroxide to the phosphorus center leading to hydrolytic cleavage of the phosphorus–ester bond.^{4,67} Nevertheless, several crucial aspects are still uncertain, such as the binding mode of the substrate in the active site prior to the hydrolysis, the effective role of each metal atom, and also the function of the two histidine residues located in the second-shell ligands (His 202 and His 296).^{4,5,7,37,46,48,58,64,67}

In order to better characterize the several steps of the catalytic mechanism of the Fe(III)–Zn(II)–PAP (from rkbPAP), for the first time a detailed theoretical exploration of the hydrolysis process is reported in this work, providing characterization of the transition states and intermediates involved and presenting the potential energy profiles for the reaction in different environments (gas phase, protein environment, and water). Moreover our computations can give insights into some interesting aspects. In particular: (i) Two models of enzyme–substrate (ES) with different orientations of the substrate into the active site were tested to evaluate the possible roles played by the conserved histidine residues (His 202 and His 296); (ii) Different protonation states of the substrate were taken into account in order to reproduce different pH values and to verify its influence on the catalytic efficiency and on the substrate binding mode; (iii) The metals role in each step of the catalytic mechanism was elucidated.

2. Computational Details and Models

The theoretical investigation of the catalytic mechanism of the Fe(III)–Zn(II)–PAP was performed at density functional theory (DFT) level by means of GAUSSIAN 03⁶⁸ suite of programs. Geometry optimizations in the gas phase were carried out using the hybrid B3LYP functional, composed by Becke's⁶⁹ three-parameter hybrid exchange functional (B3), and the correlation functional of Lee, Yang and Parr (LYP)⁷⁰ using 6-31G(d,p) basis sets for all atoms except the iron and Zn ions, which were described by the quasi-relativistic Stuttgart–Dresden pseudopotentials.⁷¹ In order to confirm proper convergence to equilibrium and transition-state geometries, vibrational frequency analysis was done based on analytical second derivatives of the Hamiltonian at the same level of theory. Solvent effects were introduced in the framework of the self-consistent reaction field conductor-like polarizable continuum model (SCRF–CPCM),^{72,73} using two dielectric constants to simulate water and reproduce the protein environment. For the latter, an empirical

value of $\epsilon = 4$ accounts for the average effect of both the protein and the water medium surrounding the protein. For the water, $\epsilon = 80$ was used. In the CPCM method, the continuum is modeled as a conductor, instead of a dielectric. This simplifies the electrostatic computations, and corrections are made a posteriori for dielectric behavior. The UA0 radii were used to build the cavity.⁷⁴ In order to obtain more accurate energies in the gas phase, in the protein environment, and in water, single points calculations were performed on the optimized geometries using the larger basis set 6-311+G(2d,2p) and testing several exchange–correlation functionals (B3LYP,^{69,70} PBEOPBE,⁷⁵ BB1K,⁷⁶ MPWB1K,⁷⁷ and MW1B95).⁷⁷ Our benchmark reported in Section 3.3, shows that the meta-hybrid functional (BB1K, MPWB1K, MW1B95) reproduces with good accuracy experimental values found on similar reactions catalyzed by PAPs enzymes.^{24,78,79} In addition, many studies have demonstrated that the hybrid-meta generalized gradient approximation (GGA) methods give more reliable results in the reproduction of the reaction kinetics showing great ability in the calculation of barrier heights with high accuracy, also compared to higher-level post-Hartree–Fock methods, supporting our evidence.^{80,81} The energy values discussed in the text are those obtained with the hybrid-meta MPWB1K functional, previously employed successfully also in other enzymatic studies.^{80–82} The crystal structure of red kidney bean PAP, determined in the presence of phosphate acting as an inhibitor (PDB code 4kbp, chain A),⁵⁶ was used to devise a model of the active site of the enzyme. The latter contains the metal ions Fe(III) and Zn(II) and the seven amino acids of their first-shell ligands. In particular, the Fe(III) ion is coordinated to Asp 135, Tyr 167, His 325, and Asp 164 that bridges both of the metals, while the Asn 201, His 286, and His 323 represent the divalent metal ion Zn(II) ligands. In order to study their roles in the catalytic cycle, two histidine residues (His 296 and His 202) of the second shell of the ligands were also included in the model. No water molecule was introduced to complete the coordination environment of the Zn ion because the formation of the precatalytic complex has been suggested to cause the expulsion of this labile terminal water ligand.⁶⁷ Only the side chains of the residues were kept in our model. Moreover the carbon atoms where truncation was done were kept fixed to their X-ray crystal positions during the optimizations to avoid an unrealistic expansion of the cluster during the calculations. This procedure gives rise to smaller imaginary frequencies, but the latter does not significantly contribute to the zero point energies (ZPE) and can thus be tolerated. A bridging hydroxide as a nucleophile was included in the cluster model, in agreement with previous studies that support the presence of this group.^{58,61} In the absence of crystallographic data for the ES complex, the latter was modeled in the active site as methyl-phosphate since this kind of enzyme catalyzes the hydrolysis of monophosphates. The resulting cluster contains 114 atoms. In order to establish the most stable spin multiplicity of the system, preliminary calculations on the ES complex with different values of spin multiplicity ($2S + 1 = 2, 4, 6$, and 8) were performed. The lowest energy was obtained with a value of 6, which arises from a high-spin

configuration of the Fe(III) center, in agreement with electron paramagnetic resonance (EPR) measurements that support our result.²⁵ The doublet, quartet, and octet electronic states lie at 36.3, 23.8, and 98.3 kcal/mol with respect to the same structure obtained with sextet multiplicity, respectively. For the quartet spin state, the entire catalytic cycle was reproduced in order to consider eventual involvement of different spin states along the potential energy surface (PES). The results clearly show that no crossing occurs between the two energetic profiles. (See Figure S1 in the Supporting Information). Spin density distribution and molecular orbital pictures for all the stationary points along the PES are reported in Figures S2 and S3 of the Supporting Information, respectively. As expected, from these data, it is clear that the higher spin densities are localized on the iron center.

3. Results and Discussion

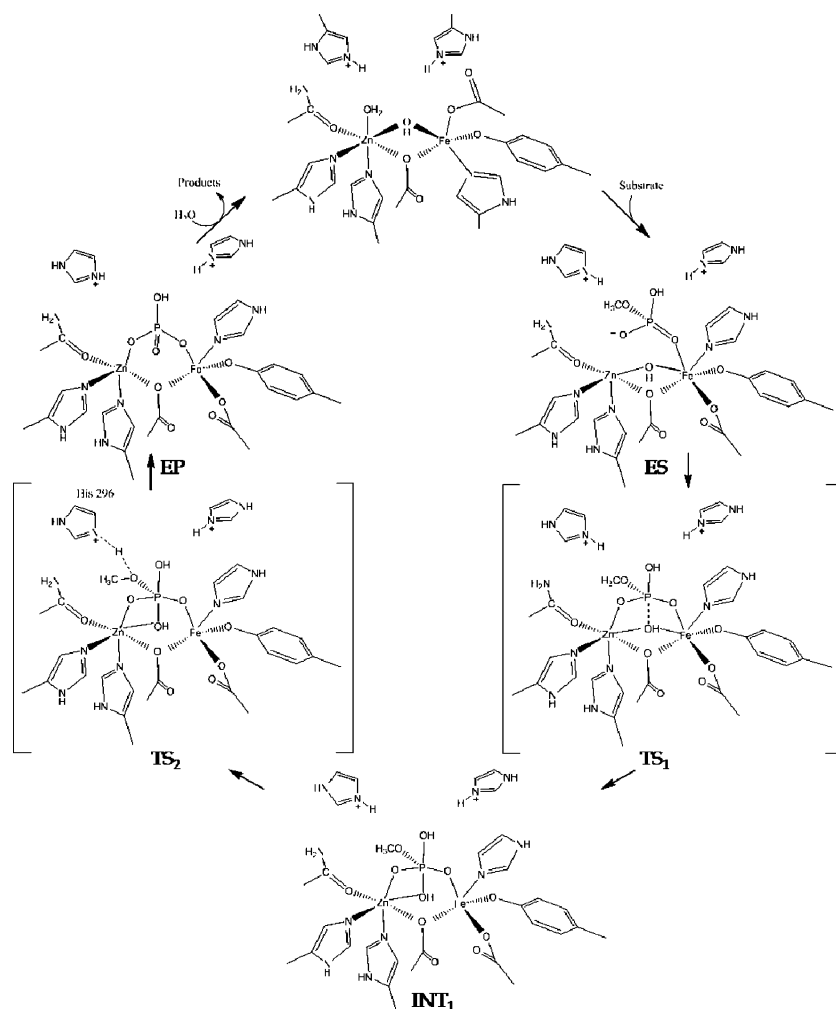
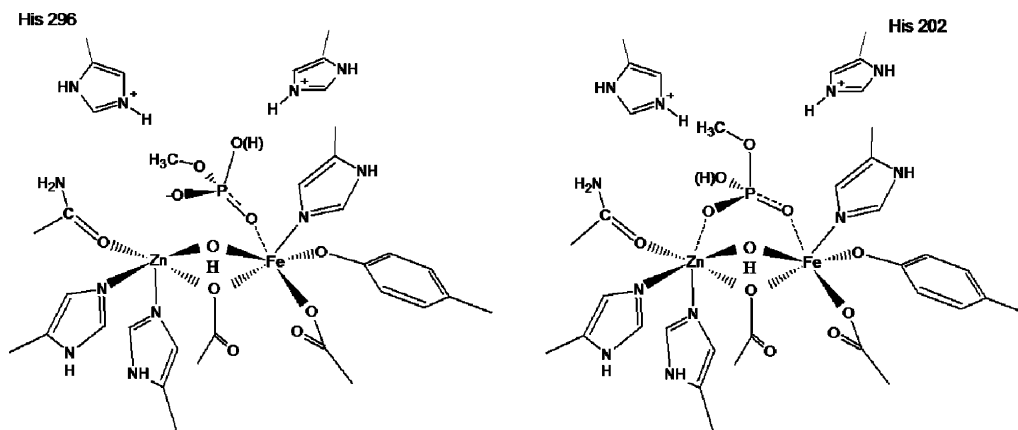
The steps involved in the whole process and determined through our calculations are sketched in Scheme 2. According to our results, a mechanism in which the metal-bridging hydroxide performs a nucleophilic attack on the phosphorus atom leading to the cleavage of the ester bond, activated by a proton shift from the histidine residue 296, is proposed. The potential energy profiles for the considered reaction cycle are depicted in Figure 5 of Section 3.3.

The possibility of a concerted SN_2 mechanism has also been considered in our investigation, but we found that two transition states are required to complete the catalytic process.

3.1. ES Complex. Since the X-ray structure of rkbPAP used to devise the cluster model of the active site was determined in the presence of an inhibitor, to obtain a valid initial structure for our exploration of the catalytic mechanism, we evaluated several crucial aspects in the construction of our model. First of all, the substrate's orientation into the active site, and then its protonation state and the coordination binding mode to the dimetallic center. In order to consider the right orientation of the substrate into the catalytic cavity, we took into account some experimental indications suggesting that the His 296 may be responsible for the proton shift to the leaving group during the catalytic cycle, while a second conserved residue His 202 should be involved only in the transition-state stabilization.^{14,65,66} According to this evidence, the substrate was modeled in the catalytic cavity with the methoxy group oriented toward the His 296 (Scheme 3a). In addition, we tried to study a mechanism in which the His 202 worked as proton carrier to the leaving group, considering the other stereoisomer of the methyl phosphate (Scheme 3b), but all the efforts to locate the saddle points for the reaction with that model failed.

From geometric point of view, the results obtained using models (a) and (b) show an important difference. The substrate binds in a different manner the dimetallic center in the optimized structures inducing different electronic distributions, probably responsible of the different activity of the two stereoisomers. The optimized ES complex for model (b) is reported in Figure S4 of the Supporting Information.

Another point of conjecture is the mode of substrate binding. Although several studies of this kind of enzyme

Scheme 2. Proposed Mechanism for the Hydrolysis of Methyl-Phosphate Promoted by Red Kidney Bean PAP**Scheme 3.** Considered Substrate Orientations into the Catalytic Cavity

exists, the exact coordination of the substrate to the dimetallic center it is still uncertain. It has been previously proposed that the precise substrate coordination may be pH dependent.⁴ In order to better understand this aspect, we took into consideration that the Fe–Zn–PAP from red kidney beans display a maximum catalytic rate at pH ≈ 6.⁷⁸ At that value of pH (4.5 < pH < 6.5), our substrate is likely in its monoanionic form ($\text{CH}_3\text{HPO}_4^-$). At pH slightly higher, the substrate could be present in its dianionic form. In order to provide insight into this important point of controversy, we

tested two different protonation states of the substrate into the active site. We were able to verify that the activation barrier associated with the model containing $\text{CH}_3\text{OPO}_3^{2-}$ as the substrate is higher by more than 10 kcal/mol with respect to the other one relative to the monoanionic species, confirming that the reaction proceeds faster at a lower pH. Moreover, we prove that the pH influences the coordination mode. The $\text{CH}_3\text{HPO}_4^-$ substrate binds in a monodentate-like manner the bimetallic center, while the dianionic form of the substrate $\text{CH}_3\text{OPO}_3^{2-}$ results in a bicoordinated ES

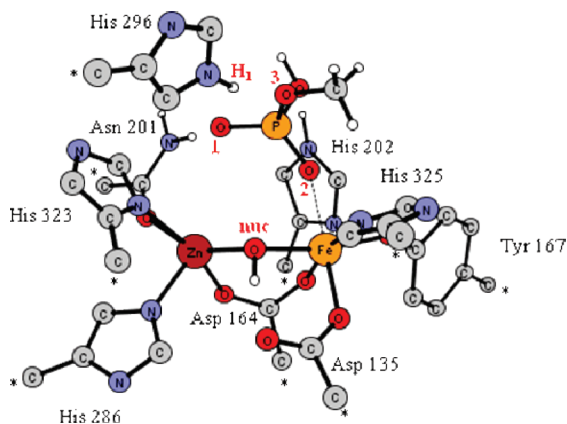


Figure 1. Optimized structure of the ES complex. Only the most significant hydrogen atoms are reported. Stars indicate the atoms kept fixed to their crystallographic positions during optimizations.

Table 1. Main Bond Lengths (\AA) of the Optimized Stationary Points along the Reaction Path

	ES	TS ₁	INT ₁	TS ₂	EP
Zn—O ₁	3.47	2.10	2.03	2.03	1.97
Fe—O ₂	2.30	2.11	2.00	2.01	2.07
Zn—Onuc	1.98	2.28	2.17	2.17	—
Fe—Onuc	2.01	2.24	3.36	3.43	—
P—Onuc	3.64	2.00	1.85	1.80	1.55
Fe—Zn	3.54	4.00	4.58	4.83	4.36
O ₃ —H ₁	1.74	1.66	1.76	1.20	0.98

complex (see Figure S5 of the Supporting Information). As a result of this preliminary investigation, we report in Figure 1 the optimized structure of the ES complex. Main geometrical parameters of ES, together with those for the other stationary points encountered along the reaction path, are collected in Table 1.

As shown in Figure 1, the overall geometry of the metal centers predicted by our calculation is of a distorted square pyramidal geometry for the pentacoordinated Zn(II) cation, while the iron center adopts an octahedral geometry. The internuclear distance between the two metal ions is 3.54 Å. In the optimized complex, the substrate is stabilized in the active site by a network of hydrogen-bonding interactions with the Asn 201 and with conserved histidine residues located in the second coordination sphere (His 202 and His 296). The distance between the bridging hydroxide and the phosphorus atom of the incoming substrate is 3.64 Å. Thanks to this disposition in the active site, the substrate is in an ideal near-attack configuration.⁸³ During the optimization, the substrate orients the methoxy group toward the protonated His 296, resulting in a monodentate coordination to the Fe(III) ion. In such a complex, the leaving group is optimally oriented along the axis of the access channel to easily leave the active site after the hydrolysis process. In Figure 2 is shown the orientation of the methoxy group with respect to the whole chain A of the enzyme.

3.2. Reaction Mechanism. The nucleophilic attack of the bridging hydroxide (O_{nuc}) to the substrate phosphorus atom (TS₁) induces a cascade of geometric changes leading to the first enzyme–intermediate complex (INT₁). The subsequent proton shift from the His 296 to the leaving group (TS₂)

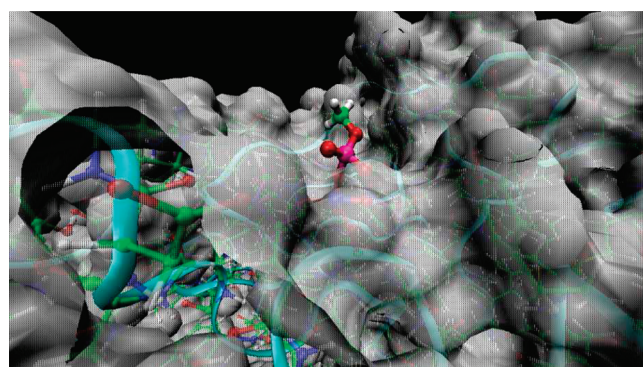


Figure 2. Orientation of the methyl phosphate group into the enzymatic channel. The B3LYP-optimized coordinates of the active site were introduced in the crystallographic data of the rkbPAP (pdb code 4kbp) by superimposition of the carbon atoms kept fixed to their X-ray crystal positions during the optimizations.

culminates in the enzyme–product complex (EP). The geometries of the optimized stationary points (see Table 1) are displayed in Figure 3.

The first transition state (TS₁) involves not only the shortening of the P—O_{nuc} distance, which in the ES varies from 3.64 to 2.00 Å but implies also important changes in the substrate coordination mode to the active site. The methyl-phosphate group binds now in a bidentate manner the dimetallic center, displaying distances of 2.10 and 2.11 Å from Zn and Fe, respectively. The bridging coordination geometry adopted led to an elongation of the Zn–Fe distance from 3.54 Å in the ES complex to 4.00 Å in the TS₁, consenting to increase the nucleophilicity of the metal-bound hydroxide by lengthening the distances Zn—O_{nuc} and Fe—O_{nuc} to 2.28 and 2.24 Å, respectively. In addition, modification in the substrate geometry was observed. The three oxygen atoms of the substrate (O₁, O₂, and O₃) occupy equatorial positions with respect to P, adopting a pentacoordinate geometry. The analysis of the vibrational mode clearly indicates the stretching of the incoming P—O_{nuc} bond, as a result of the nucleophilic attack of the bridging hydroxide to the phosphorus atom, and was confirmed to be a first-order saddle point with only one imaginary frequency (88 cm⁻¹). The hydrogen-bonding network found in the enzyme–substrate complex is still retained in the transition state. In particular the distance between the leaving group's oxygen atom and the hydrogen of the conserved His 296 (O₃—H₁) decreases in the transition state, reaching a distance of 1.66 Å. The latter not only contributes to stabilize the transition state but allows an optimal orientation of the leaving group toward the subsequent protonation step. TS₁ lies at 15.6 kcal/mol above ES, as can be observed from Figure 5. Upon addition of solvent effects, the barrier becomes slightly lower (13.1 and 13.3 kcal/mol for protein environment and water, respectively).

A trigonal bipyramidal geometry was found for the phosphorus atom in the intermediate complex (INT₁) in which the P—O_{nuc} bond is completely formed being 1.85 Å. This mode of coordination has been observed in the crystal

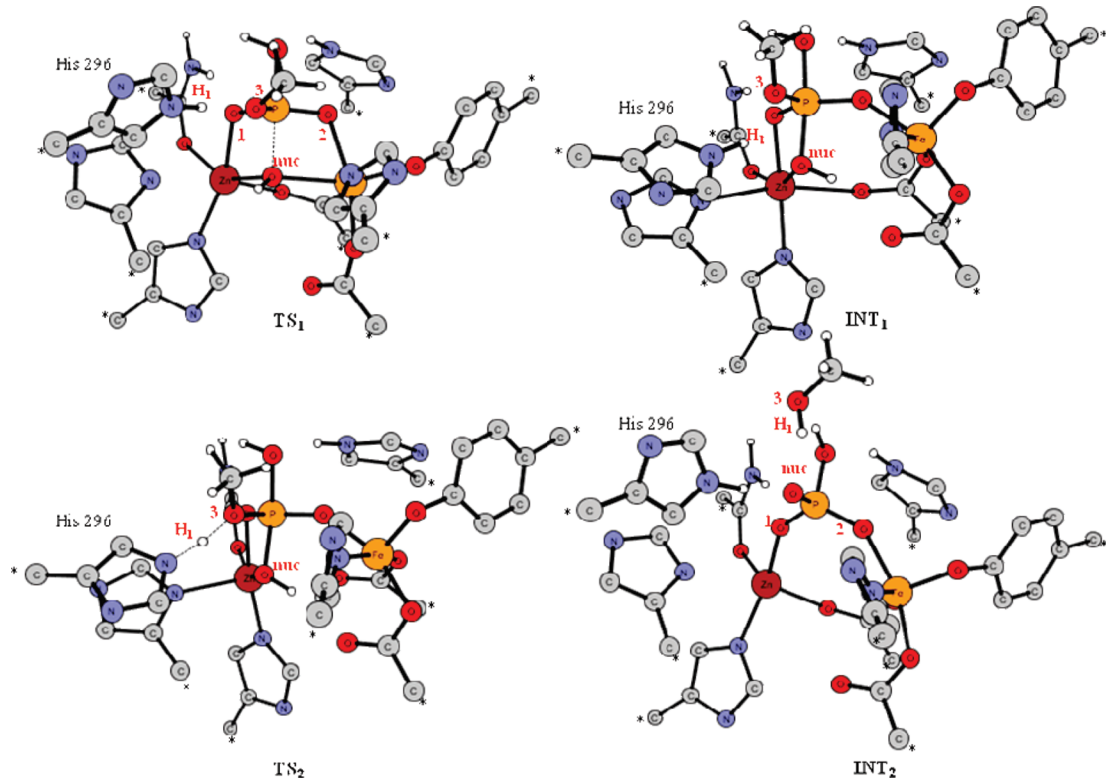


Figure 3. Optimized structures of the stationary points TS_1 , INT_1 , TS_2 , and EP for the hydrolysis of the methyl phosphate promoted by the rkbPAP enzyme. Stars indicate the atoms kept fixed to their crystallographic positions during optimizations. Only the most significant hydrogen atoms are reported in the figure.

structures of sweet potato PAP⁷⁸ and di-Ni(II) urease,⁸⁴ both with bound phosphate, and of di-Mn(II) λ PP,⁸⁵ with bound sulfate.

Although the substrate remains still bicoordinated to the dimetallic center, the distance between the Zn and Fe ions increases significantly becoming 4.58 Å. The lengthening of the metal–metal distance was already suggested in a previous work, in which the binding of the substrate has been shown to decrease the coupling interaction between the two metal centers, as indicated by a decrease in J from 20 to 6 cm⁻¹.⁵⁸ The bridging hydroxide is completely shifted away from the trivalent metal ion toward the divalent one, showing distances of 3.36 and 2.17 Å from them, respectively. From an energetic point of view, in both the gas phase and the solvent, the intermediate INT_1 shows only a small difference in the energy values with respect to TS_1 .

To get the final product, a proton shift from the His 296 to the substrate's methylated oxygen atom was observed in the second transition state TS_2 . An imaginary frequency of $376i\text{ cm}^{-1}$ confirms its nature as first-order saddle point. The vibrational mode indicates the motion of the N–H₁ and H₁–O₃ couple of bonds with critical lengths of 1.27 and 1.20 Å, respectively. In such a transition state, the proton shift happens before the just formed methanol group leaves the substrate. This stationary point lies at 19.3 kcal/mol above ES in the gas phase, while solvation effects increase this difference becoming 21.0 and 22.7 kcal/mol in protein environment and water, respectively. The requirement of an activated leaving group to reach an optimal catalytic efficiency has been the subject of previous studies.^{78,24} For red kidney bean and pig PAP, it was demonstrated that

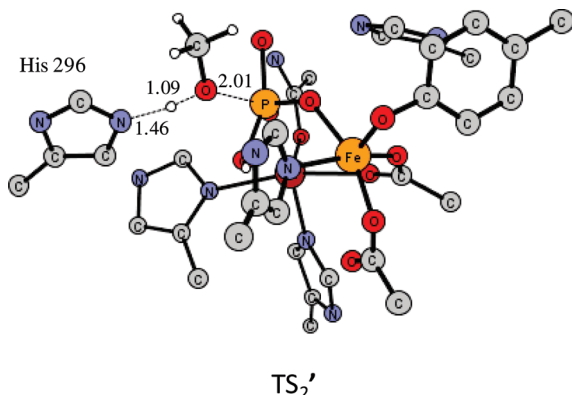


Figure 4. Concerted transition state in which the release of the methoxy group occurs at the same time of the proton shift from the His 296

reactivity declines as the leaving group's pK_a increases, while no dependence of catalytic parameters from the leaving group's pK_a was found from the sweet potato PAP. This evidence suggests that sweet potato PAP can catalyze efficiently a range of activated and inactivated phosphate esters in contrast to red kidney bean and pig PAPs. The possibility that the bond between the phosphorus atom and the methoxy group breaks without activation was also considered in our investigation. We were able to characterize a further transition state (TS_2') in which no activation takes place before the leaving group leaves and in which a shift from the His 296 occurs in a concerted manner with the scission (Figure 4). The analysis of the obtained vibrational frequency ($138i\text{ cm}^{-1}$) clearly indicates the rupture of the

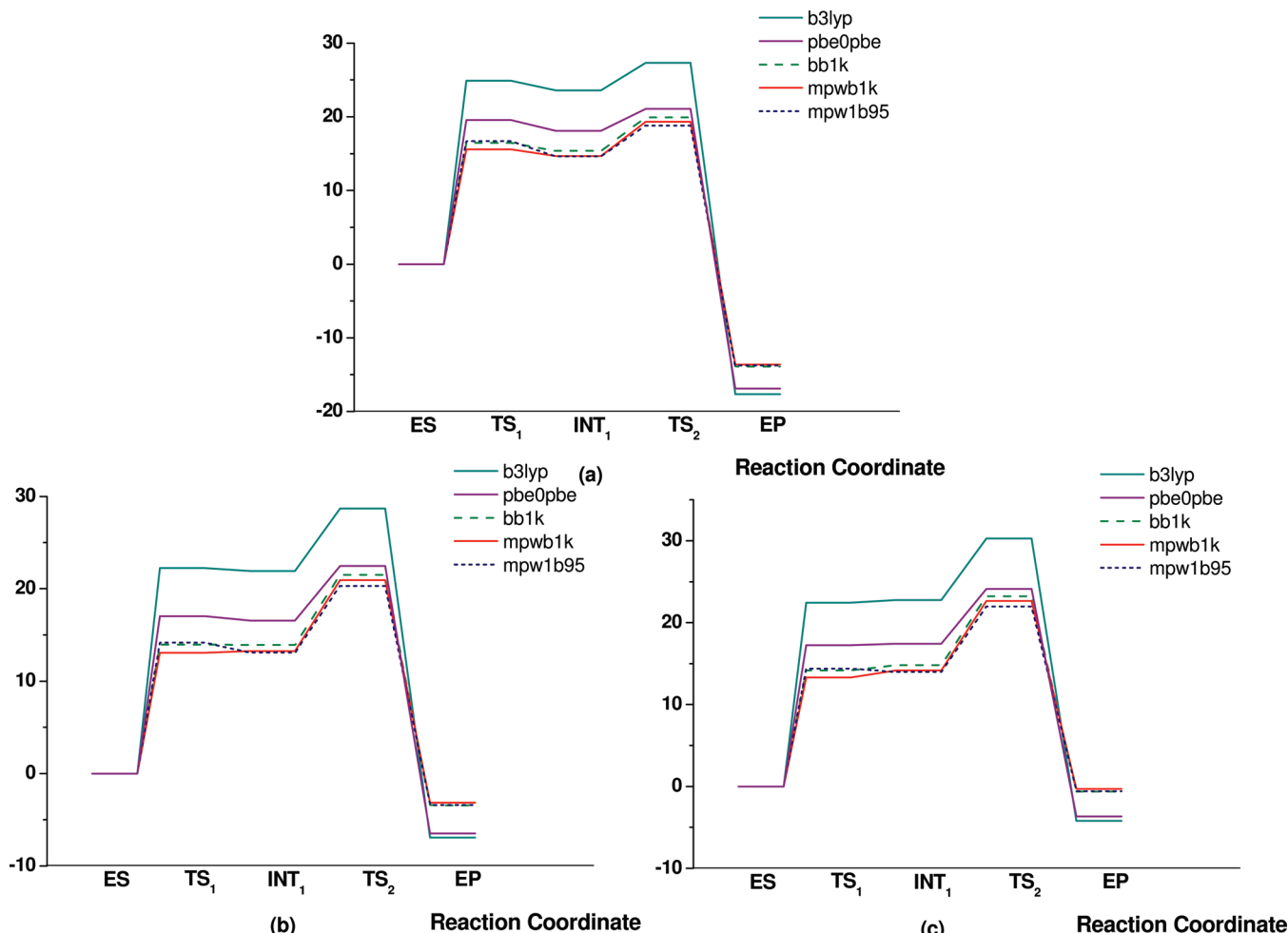


Figure 5. Potential energy profiles for the reaction in: (a) gas phase, (b) protein environment ($\epsilon = 4$), and (c) water.

P–O₃ bond and the formation of the O₃–H₁ one. Nevertheless, this hypothesis of a concerted transition state is energetically unfavorable requiring a higher amount of energy with respect to the other transition state TS₂. This stationary point lies at 32.0 kcal/mol with respect to the ES in the gas phase, while with the introduction of solvent effects, the differences become 36.8 and 39.0 kcal/mol in protein environment and water. According to our calculation for red kidney bean PAP, we can observe that the activation of the leaving group is crucial to get the final enzyme–product complex.

The last point encountered along the reaction path corresponds to the enzyme–product complex (EP). The release of the leaving group induces significant structural rearrangements. The phosphorus atom is likely to regenerate its optimal tetrahedral geometry requiring a reorganization of the active site. During the optimization, a rotation of the bond between the phosphorus atom and the native nucleophile (P–O_{nuc}) occurs to reach a reasonable tetra-coordination. The phosphate remains tightly bound to the dimetallic center by the oxygen atoms O₁ and O₂ and with distances of 1.97 and 2.07 Å from Zn and Fe, respectively. The OH_{nuc} group oriented toward the His 296 spontaneously transfers the proton to the His 296, regenerating the active site. The distance between the metal ions decreases in the EP complex reaching 4.36 Å, from 4.83 Å in the previous TS₂ geometry.

Such a complex is stabilized by a network of hydrogen bonding involving the His 296 and His 202 of the second coordination sphere, the His 325 Fe(III)-bound, and Asn 201 Zn(II)-bound. The EP complex is obtained exothermically with a great energy gain (13.6 kcal/mol in gas phase). Interestingly, the solvent effect seems to destabilize the product of reaction that is found at –3.1 and –0.3 kcal/mol lower in energy than the reactants.

3.3. Energetic of the Reaction. Different exchange–correlation functionals were used to estimate the energies of the stationary points located on the paths in the gas phase and in different environments (water and protein). This benchmark could be interesting since a large number of density functionals at different levels of sophistication have become available, and a well-established computation protocol for the enzymatic reaction is still lacking.

A detailed analysis of the performance of the popular B3LYP functional in the reproduction of a large variety of chemical properties and system types was performed in a recent study.⁸⁰ The latter shows that the B3LYP performance in the prediction of geometrical structures including closed- and open-shell structures is satisfactory and is able to compete in accuracy with the other proposed XC functional as well as with other ab initio methods.

On the contrary, for some properties several new density functionals significantly outperform this popular hybrid

Table 2. Energies (kcal/mol) of the Stationary Points along the Reaction Paths^a

		ES	TS ₁	INT ₁	TS ₂	EP
$\epsilon = 4$	B3LYP	0	24.93	23.58	27.33	-17.65
	PBE0PBE	0	19.58	18.11	21.07	-16.87
	BB1K	0	16.47	15.36	19.92	-13.91
	MPWB1K	0	15.59	14.66	19.34	-13.64
	MPW1B95	0	16.68	14.61	18.83	-13.76
	B3LYP	0	22.26	21.94	28.67	-6.94
	PBE0PBE	0	17.03	16.55	22.48	-6.48
	BB1K	0	13.94	13.92	21.52	-3.45
	MPWB1K	0	13.06	13.24	20.96	-3.14
	MPW1B95	0	14.16	13.09	20.32	-3.39
$\epsilon = 80$	B3LYP	0	22.44	22.77	30.27	-4.18
	PBE0PBE	0	17.24	17.42	24.11	-3.67
	BB1K	0	14.17	14.82	23.22	-0.62
	MPWB1K	0	13.3	14.15	22.67	-0.3
	MPW1B95	0	14.39	13.97	21.98	-0.57

^a In the gas phase, in the protein environment ($\epsilon = 4$), and in water ($\epsilon = 80$).

functional. Many studies have demonstrated that the hybrid-meta GGA methods give more reliable results in the reproduction of the reaction kinetics showing great ability in the calculation of barrier heights with high accuracy.⁸⁰ Taking these aspects under consideration, in our investigation we chose the B3LYP functional for the optimizations of all the stationary points along the reaction path and, to obtain energetic values, we performed single point calculation with a larger basis set testing the hybrids B3LYP and PBE0PBE and the meta-hybrids BB1K, MPWB1K, and MW1B95. The results are shown in Figure 5.

From Table 2 and Figure 5 it is possible to observe that the hybrid-meta GGA functionals (BB1K, MPWB1K, and MPW1B95) give very similar results concerning the energy of the stationary points along the paths in the gas phase, in the protein environment, and in water. In addition, the calculated values well agree with the energy barriers extracted from the k_{cat} experimentally obtained for reactions catalyzed by PAPs enzymes (13–15 kcal/mol depending on the substrate).^{24,78,79}

On the contrary, the profiles obtained at B3LYP and PBE0PBE levels of theory show higher energy results. Furthermore, we can observe that the protein environment has a slightly higher stabilization effect on the structures than the more polar water environment, and moreover only the first part of the mechanism results stabilized. The TS₂ and the product of the reaction seem to be destabilized with the introduction of the environment.

Conclusion

The catalytic mechanism of the Fe(III)–Zn(II) purple acid phosphatase (PAP) enzyme was investigated at the density functional (DF) level of theory. The model cluster used to simulate the active site of the enzyme, made up of 114 atoms, was large enough to reliably reproduce the hydrolysis of the methyl-phosphate monoanionic substrate ($\text{CH}_3\text{OPO}_3^{2-}$).

The main results can be summarized as follows:

- The PAP hydrolysis reaction involves the formation of the trigonal bipyramidal intermediate, arising from nucleophilic addition of the bridging hydroxide molecule

to the substrate phosphorus atom, followed by the protonation of the substrate methoxy group leading to the final P–O bond cleavage.

- The role of the two conserved histidine residues was elucidated. The protonated His 296 has been confirmed to play a fundamental role acting as a proton carrier and activating the methoxy leaving group, while the His 202 takes part in the optimal orientation of the substrate during the catalysis by establishing a hydrogen bond with it.
- From our study emerges that the rate-limiting step of the reaction is the nucleophilic attack followed by the less energetically demanding release of the leaving group.
- We were able to establish that the activation of the leaving group by the His 296 is actually crucial in order to reach an optimal catalytic efficiency. A transition state (TS_{2'}) in which no activation takes place before the leaving group leaves and in which a shift from the His 296 occurs in a concerted manner with the scission was further characterized, but it requires a higher amount of energy to be overcome than TS₂.
- The dianionic form of the substrate was also considered in our investigation. We found that the activation barrier for the nucleophilic attack associated with that model is considerably higher than the other one relative to the monoanionic species, confirming that the reaction proceeds faster at lower pH. This result is in agreement with the experimental indications that support a monoanionic substrate being pH = 6, the optimum value for the achievement of the maximum catalytic rate for rkbPAP.⁷⁸
- We found that the monoanionic form of methylphosphate binds in a monodentate-like manner, the bimetallic center in the precatalytic complex, while the dianionic form $\text{CH}_3\text{OPO}_3^{2-}$ results in a bicoordinated ES complex. Our evidence supports the hypothesis that the mode of substrate binding is pH dependent, as it has been previously suggested in other works.⁴
- Different XC functionals were used to calculate the barrier heights in the gas phase, in the protein environment, and in water. The meta-hybrid functionals give results that better agree with the energy barriers calculated from the k_{cat} obtained for similar reactions catalyzed by PAPs enzymes, confirming their ability in the reproduction of the reaction kinetics.

Acknowledgment. The University of Calabria, the Regione Calabria (FSE-POR 2000/2006, misura 3.7), the MIUR PRIN 2008, and the University of Porto are gratefully acknowledged.

Supporting Information Available: Further information regarding the chosen spin state along the PES, spin density distribution, and molecular orbital picture for the all stationary points, optimized structure, and selected geometrical parameters of the ES complex using Model (b), and the ES and TS₁ containing $\text{CH}_3\text{OPO}_3^{2-}$ substrates are provided. This information are available free of charge via the Internet at <http://pubs.acs.org/>.

References

- (1) Twitchett, M. B.; Sykes, A. G. *Eur. J. Inorg. Chem.* **1999**, 2105.
- (2) Klabunde, T.; Krebs, B. *Struct. Bonding (Berlin, Ger.)* **1997**, 89, 177.
- (3) Oddie, G. W.; Schenk, G.; Angel, N. Z.; Walsh, N.; Guddat, L. W.; de Jersey, J.; Cassady, A. I.; Hamilton, S. E.; Hume, D. A. *Bone* **2000**, 27, 575.
- (4) Mitić, N.; Smith, S. J.; Neves, A.; Guddat, L. W.; Gahan, L. R.; Schenk, G. *Chem. Rev.* **2006**, 106, 3338.
- (5) Wilcox, D. E. *Chem. Rev.* **1996**, 96, 2435.
- (6) Sträter, N.; Lipscomb, W. N.; Klabunde, T.; Krebs, B. *Angew. Chem., Int. Ed. Engl.* **1996**, 35, 2024.
- (7) Dismukes, G. C. *Chem. Rev.* **1996**, 96, 2909.
- (8) Barford, D.; Das, A. K.; Egloff, M. P. *Annu. Rev. Biophys. Biomol. Struct.* **1998**, 27, 133.
- (9) Rusnak, F.; Mertz, P. *Physiol. Rev.* **2000**, 80, 1483.
- (10) Jackson, M. D.; Denu, J. M. *Chem. Rev.* **2001**, 101, 2313.
- (11) Lowther, W. T.; Matthews, B. W. *Biochim. Biophys. Acta* **2000**, 1477, 157.
- (12) Nuttelman, P. R.; Roberts, R. M. *J. Biol. Chem.* **1990**, 265, 12192.
- (13) Sibille, J. C.; Doi, K.; Aisen, P. *J. Biol. Chem.* **1987**, 262, 59.
- (14) Kaija, H.; Alatalo, S. L.; Halleen, J. M.; Lindqvist, Y.; Schneider, G.; Väänänen, H. K.; Vihko, P. *Biochem. Biophys. Res. Commun.* **2002**, 292, 128.
- (15) Räisänen, S. R.; Alatalo, S. L.; Ylipahkala, H.; Halleen, J. M.; Cassady, A. I.; Hume, D. A.; Väänänen, H. K. *Biochem. Biophys. Res. Commun.* **2005**, 331, 120.
- (16) Moss, D. W.; Raymond, F. D.; Wile, D. B. *Crit. Rev. Clin. Lab. Sci.* **1995**, 32, 431.
- (17) Angel, N. Z.; Walsh, N.; Forwood, M. R.; Ostrowski, M. C.; Cassady, A. I.; Hume, D. A. *J. Bone Miner. Res.* **2000**, 15, 103.
- (18) Hayman, A. R.; Jones, S. J.; Boyde, A.; Foster, D.; Colledge, W. H.; Carlton, M. B.; Evans, M. J.; Cox, T. M. *Development* **1996**, 122, 3151.
- (19) Ek-Rylander, B.; Flores, M.; Wendel, M.; Heinegard, D.; Andersson, G. *J. Biol. Chem.* **1994**, 269, 14853.
- (20) Valizadeh, M.; Schenk, G.; Nash, K.; Oddie, G. W.; Guddat, L. W.; Hume, D. A.; de Jersey, J.; Burke, T. R., Jr.; Hamilton, S. *Arch. Biochem. Biophys.* **2004**, 424, 154.
- (21) Cashikar, A. G.; Kumaresan, R.; Rao, N. M. *Plant Physiol.* **1997**, 114, 907.
- (22) Antanaitis, B. C.; Aisen, P. *J. Biol. Chem.* **1982**, 257, 5330.
- (23) Doi, K.; Bradley, C.; Aisen, P. *Struct. Bonding (Berlin, Ger.)* **1988**, 70, 1.
- (24) Schenk, G.; Ge, Y.; Carrington, L. E.; Wynne, C. J.; Searle, I. R.; Carroll, B. J.; Hamilton, S.; de Jersey, J. *Arch. Biochem. Biophys.* **1999**, 370, 183.
- (25) Durmus, A.; Eicken, C.; Sift, B. H.; Kratel, A.; Kappi, R.; Hüttermann, J.; Krebs, B. *Eur. J. Biochem.* **1999**, 260, 709.
- (26) Merkx, M.; Averill, B. A. *Biochemistry* **1998**, 37, 8490.
- (27) Chen, T. T.; Bazer, F. W.; Cetorelli, J. J.; Pollard, W. E.; Roberts, R. M. *J. Biol. Chem.* **1973**, 248, 8560.
- (28) Campbell, H. D.; Zerner, B. *Biochem. Biophys. Res. Commun.* **1973**, 54, 1493.
- (29) Campbell, H. D.; Dionysius, D. A.; Keough, D. T.; Wilson, B. E.; de Jersey, J.; Zerner, B. *Biochem. Biophys. Res. Commun.* **1978**, 82, 615.
- (30) Robinson, D. B.; Glew, R. H. *J. Biol. Chem.* **1980**, 255, 5864.
- (31) Hayman, A. R.; Warburton, M. J.; Pringle, J. A.; Coles, B.; Chambers, T. *J. Biochem. J.* **1989**, 261, 601.
- (32) Allen, S. H.; Nuttelman, P. R.; Ketcham, C. M.; Roberts, R. M. *J. Bone Miner. Res.* **1989**, 4, 47.
- (33) Janckila, A. J.; Woodford, T. A.; Lam, K. W.; Li, C. Y.; Yam, L. T. *Leukemia* **1992**, 6, 199.
- (34) Beck, J. L.; McConachie, L. A.; Summors, A. C.; Arnold, W. N.; de Jersey, J.; Zerner, B. *Biochim. Biophys. Acta* **1986**, 869, 61.
- (35) Bozzo, G. G.; Raghothama, K. G.; Plaxton, W. C. *Biochem. J.* **2004**, 377, 419.
- (36) Bozzo, G. G.; Raghothama, K. G.; Plaxton, W. C. *Eur. J. Biochem.* **2002**, 269, 6278.
- (37) Schenk, G.; Bouthard, C. L.; Carrington, L. E.; Noble, C. J.; Moubaraki, B.; Murray, K. S.; de Jersey, J.; Hanson, G. R.; Hamilton, S. *J. Biol. Chem.* **2001**, 276, 19084.
- (38) Schenk, G.; Guddat, L. W.; Ge, Y.; Carrington, L. E.; Hume, D. A.; Hamilton, S.; de Jersey, J. *Gene* **2000**, 250, 117.
- (39) Antanaitis, B. C.; Aisen, P.; Lilienthal, H. R. *J. Biol. Chem.* **1983**, 258, 3166.
- (40) Averill, B. A.; Davis, J. C.; Burman, S.; Zirino, T.; Sanders-Loehr, J.; Loehr, T. M.; Sage, J. T.; Debrunner, P. G. *J. Am. Chem. Soc.* **1987**, 109, 3760.
- (41) Yang, Y.-S.; McCormick, J. M.; Solomon, E. I. *J. Am. Chem. Soc.* **1997**, 119, 11832.
- (42) Wang, D. L.; Holz, R. C.; David, S. S.; Que, L.; Stankovich, M. T. *Biochemistry* **1991**, 30, 8187.
- (43) Bernhardt, P. V.; Schenk, G.; Wilson, G. J. *Biochemistry* **2004**, 43, 10387.
- (44) Beck, J. L.; Keough, D. T.; de Jersey, J.; Zerner, B. *Biochim. Biophys. Acta* **1984**, 791, 357.
- (45) Funhoff, E. G.; Ljusberg, J.; Wang, Y.; Andersson, G.; Averill, B. A. *Biochemistry* **2001**, 40, 11614.
- (46) Funhoff, E. G.; Klaassen, C. H. W.; Samyn, B.; Van Beeumen, J.; Averill, B. A. *ChemBioChem* **2001**, 2, 355.
- (47) Merkx, M.; Averill, B. A. *Biochemistry* **1998**, 37, 11223.
- (48) Merkx, M.; Pinkse, M. W. H.; Averill, B. A. *Biochemistry* **1999**, 38, 9914.
- (49) Pinkse, M. W. H.; Merkx, M.; Averill, B. A. *Biochemistry* **1999**, 38, 9926.
- (50) Funhoff, E. G.; Bollen, M.; Averill, B. A. *J. Inorg. Biochem.* **2005**, 99, 521.
- (51) Beck, J. L.; McArthur, M. J.; de Jersey, J.; Zerner, B. *Inorg. Chim. Acta* **1988**, 153, 39.
- (52) Beck, J. L.; de Jersey, J.; Zerner, B. *J. Am. Chem. Soc.* **1988**, 110, 3317.
- (53) Gehring, S.; Fleischhauer, P.; Behlendorf, M.; Huber, M.; Lorösch, J.; Haase, W.; Dietrich, M.; Witzel, H.; Locke, R.; Krebs, B. *Inorg. Chim. Acta* **1996**, 252, 13.

- (54) Battistuzzi, G.; Dietrich, M.; Locke, R.; Witzel, H. *Biochem. J.* **1997**, 323, 593.
- (55) Sträter, N.; Klabunde, T.; Tucker, P.; Witzel, H.; Krebs, B. *Science* **1995**, 268, 1489.
- (56) Klabunde, T.; Sträter, N.; Fröhlich, R.; Witzel, H.; Krebs, B. *J. Mol. Biol.* **1996**, 259, 737.
- (57) Klabunde, T.; Sträter, N.; Krebs, B.; Witzel, H. *FEBS Lett.* **1995**, 367, 56.
- (58) Smoukov, S. K.; Quaroni, L.; Wang, X.; Doan, P. E.; Hoffman, B. M.; Que, L., Jr. *J. Am. Chem. Soc.* **2002**, 124, 2595.
- (59) Guddat, L. W.; McAlpine, A. S.; Hume, D.; Hamilton, S.; de Jersey, J.; Martin, J. L. *Structure* **1999**, 7, 757.
- (60) Lindqvist, Y.; Johansson, E.; Kaija, H.; Vihko, P.; Schneider, G. *J. Mol. Biol.* **1999**, 291, 135.
- (61) Wang, X.; Que, L. *Biochemistry* **1998**, 37, 7813.
- (62) Merkx, M.; Averill, B. A. *J. Am. Chem. Soc.* **1999**, 121, 6683.
- (63) Merkx, M.; Averill, B. A. *Biochemistry* **1998**, 37, 8490.
- (64) Twitchett, M. B.; Schenk, G.; Aquino, M. A. S.; Yiu, D. T. Y.; Lau, T. C.; Sykes, A. G. *Inorg. Chem.* **2002**, 41, 5787.
- (65) Funhoff, E. G.; Wang, Y.; Andersson, G.; Averill, B. A. *FEBS J.* **2005**, 272, 2968.
- (66) Truong, N. T.; Naseri, J. I.; Vogel, A.; Rompel, A.; Krebs, B. *Arch. Biochem. Biophys.* **2005**, 440, 38.
- (67) Schenk, G.; Elliott, T. W.; Leung, L.; Carrington, L. E.; Mitić, N.; Gahan, L. R.; Guddat, L. W. *BMC Struct. Biol.* **2008**, 8, 6.
- (68) Frisch, M. J.; Trucks, G. W.; Schlegel, H. B.; Scuseria, G. E.; Robb, M. A.; Cheeseman, J. R.; Montgomery, J. A., Jr.; Vreven, T.; Kudin, K. N.; Burant, J. C.; Millam, J. M.; Iyengar, S. S.; Tomasi, J.; Barone, V.; Mennucci, B.; Cossi, M.; Scalmani, G.; Rega, N.; Petersson, G. A.; Nakatsuji, H.; Hada, M.; Ehara, M.; Toyota, K.; Fukuda, R.; Hasegawa, J.; Ishida, M.; Nakajima, T.; Honda, Y.; Kitao, O.; Nakai, H.; Klene, M.; Li, X.; Knox, J. E.; Hratchian, H. P.; Cross, J. B.; Bakken, V.; Adamo, C.; Jaramillo, J.; Gomperts, R.; Stratmann, R. E.; Yazyev, O.; Austin, A. J.; Cammi, R.; Pomelli, C.; Ochterski, J. W.; Ayala, P. Y.; Morokuma, K.; Voth, G. A.; Salvador, P.; Dannenberg, J. J.; Zakrzewski, V. G.; Dapprich, S.; Daniels, A. D.; Strain, M. C.; Farkas, O.; Malick, D. K.; Rabuck, A. D.; Raghavachari, K.; Foresman, J. B.; Ortiz, J. V.; Cui, Q.; Baboul, A. G.; Clifford, S.; Cioslowski, J.; Stefanov, B. B.; Liu, G.; Liashenko, A.; Piskorz, P.; Komaromi, I.; Martin, R. L.; Fox, D. J.; Keith, T.; Al-Laham, M. A.; Peng, C. Y.; Nanayakkara, A.; Challacombe, M.; Gill, P. M. W.; Johnson, B.; Chen, W.; Wong, M. W.; Gonzalez, C.; Pople, J. A. *Gaussian 03*, revision A.1; Gaussian, Inc.: Pittsburgh, PA, 2003.
- (69) Becke, A. D. *J. Chem. Phys.* **1993**, 98, 5648.
- (70) Lee, C. T.; Yang, W. T.; Parr, R. G. *Phys. Rev. B: Condens. Matter Mater. Phys.* **1988**, 37, 785.
- (71) Andrae, D.; Haussermann, U.; Dolg, M.; Stoll, H.; Preuss, H. *Theor. Chim. Acta* **1990**, 77, 123.
- (72) Barone, V.; Cossi, M. *J. Phys. Chem. A* **1998**, 102, 1995.
- (73) Cossi, M.; Rega, N.; Scalmani, G.; Barone, V. *J. Comput. Chem.* **2003**, 24, 669.
- (74) Rappe, A. K.; Casewit, C. J.; Colwell, K. S.; Goddard, W. A., III; Skiff, W. M. *J. Am. Chem. Soc.* **1992**, 114, 10024.
- (75) Adamo, C.; Barone, V. *J. Chem. Phys.* **1999**, 110, 6158.
- (76) Zhao, Y.; Lynch, B. J.; Truhlar, D. G. *J. Phys. Chem. A* **2004**, 108, 2715.
- (77) Zhao, Y.; Truhlar, D. G. *J. Phys. Chem. A* **2004**, 108, 6908.
- (78) Schenk, G.; Gahan, L. R.; Carrington, L. E.; Mitić, N.; Valizadeh, M.; Hamilton, S. E.; de Jersey, J.; Guddat, L. W. *Proc. Natl. Acad. Sci. U.S.A.* **2005**, 102, 273.
- (79) Cox, R. S.; Schenk, G.; Mitic, N.; Gahan, L. R.; Hengge, A. C. *J. Am. Chem. Soc.* **2007**, 129, 9550.
- (80) Sousa, S. F.; Fernandes, P. A.; Ramos, M. J. *J. Phys. Chem. A* **2007**, 111, 10439.
- (81) Bras, N. F.; Moura-Tamames, S. A.; Fernandes, P. A.; Ramos, M. J. *J. Comput. Chem.* **2008**, 29, 2565.
- (82) Leopoldini, M.; Russo, N.; Toscano, M. *Chem.—Eur. J.* **2009**, 15, 8026.
- (83) Hur, S.; Brulce, T. C. *Proc. Natl. Acad. Sci. U.S.A.* **2003**, 100, 12015.
- (84) Voegli, W. C.; White, D. J.; Reiter, N. J.; Rusnak, F.; Rosenzweig, A. C. *Biochemistry* **2000**, 39, 15365.
- (85) Benini, S.; Rypniewski, W. R.; Wilson, K. S.; Ciurli, S.; Mangani, S. *J. Biol. Inorg. Chem.* **2001**, 6, 778.

CT100187C